Research Square

Preprints are preliminary reports that have not undergone peer review.
They should not be considered conclusive, used to inform clinical practice,
or referenced by the media as validated information.

Rosa roxburghii-derived nanovesicles alleviate acute lung injury by reshaping the gut microbiota and regulating tryptophan-kynurenine metabolism

Yan Zeng
Zhejiang Provincial People's Hospital(Affiliated People's Hospital)
Jun Zhang
Zhejiang Provincial People's Hospital Bijie Hospital
Qin Chu
Zhejiang Provincial People's Hospital(Affiliated People's Hospital)
Ailin Wu
Zhejiang Provincial People's Hospital(Affiliated People's Hospital)
Le Ding
Zhejiang Provincial People's Hospital(Affiliated People's Hospital)
Yuanyuan Wang
Zhejiang Provincial People's Hospital(Affiliated People's Hospital)
Xin Zhang
Zhejiang Provincial People's Hospital(Affiliated People's Hospital)
Xinyun Tu
Aksu First People’s Hospital
Weijiao Fan
Zhejiang Provincial People's Hospital(Affiliated People's Hospital)
Mengqing Zheng
Zhejiang Provincial People's Hospital(Affiliated People's Hospital)
Jie Wang
EVital Bio (Hangzhou) Co.
Weidong Pan
Guizhou Medical University
Zhangfeng Zhong
City University of Macau
Xiaoru Chang
Zhejiang Provincial People's Hospital(Affiliated People's Hospital)
Xiaozhou Mou
mouxz@zju.edu.cn

Zhejiang Provincial People's Hospital(Affiliated People's Hospital)

Article

Keywords: Rosa roxburghii extracellular vesicles, acute lung injury, gut–lung axis, tryptophan metabolism, gut microbiota

Posted Date: November 24th, 2026

DOI: https://doi.org/10.21203/rs.3.rs-11337832/v1

License: This work is licensed under a Creative Commons Attribution 4.0 International License. Read Full License

Additional Declarations: No competing interests reported.

Rosa roxburghii-derived nanovesicles alleviate acute lung injury by reshaping the gut microbiota and regulating tryptophan-kynurenine metabolism

Yan Zeng[1,#], Jun Zhang[2,#], Qin Chu[1,#], Ailin Wu[1], Le Ding[3], Yuanyuan Wang[1], Xin Zhang[3], Xinyun Tu[4], Weijiao Fan[1], Mengqing Zheng[1], Jie Wang[5], Weidong Pan[7], Zhangfeng Zhong [6]*, Xiaoru Chang[3]*, Xiaozhou Mou[1]*

1 Center for Rehabilitation Medicine, Rehabilitation & Sports Medicine Research Institute of Zhejiang Province, Department of Rehabilitation Medicine, Zhejiang Provincial People's Hospital(Affiliated People's Hospital), Hangzhou Medical College, Hangzhou, Zhejiang, China.

2 Department of Orthopedics, Zhejiang Provincial People's Hospital Bijie Hospital, Bijie, Guizhou, 551700, China

3 Center for Rehabilitation Medicine, Department of Neurology, Zhejiang Provincial People's Hospital(Affiliated People's Hospital), Hangzhou Medical College, Hangzhou, Zhejiang, China.

4 Aksu First People’s Hospital, Aksu 843000, Xin jiang, China.

5 EVital Bio (Hangzhou) Co., Ltd, Hangzhou 310056, China.

6 Faculty of Health and Wellness, City University of Macau, Macao SAR 999078, China.

7 State Key Laboratory of Discovery and Utilization of Functional Components in Traditional Chinese Medicine & School of Pharmaceutical Sciences, Guizhou Medical

University, Guian New District 561113, China.

#, These authors contributed equally to this work.

Corresponding authors:

Zhangfeng Zhong Faculty of Health and Wellness, City University of Macau, Macao SAR 999078, China. Email:zfzhong@cityu.edu.mo

Xiaozhou Mou, Center for Rehabilitation Medicine, Rehabilitation & Sports Medicine Research Institute of Zhejiang Province, Department of Rehabilitation Medicine, Zhejiang Provincial People's Hospital(Affiliated People's Hospital), Hangzhou Medical College, Hangzhou, Zhejiang Province 310014, China. Email: mouxz@zju.edu.cn

Xiaoru Chang, Center for Rehabilitation Medicine, Department of Neurology, Zhejiang Provincial People's Hospital(Affiliated People's Hospital), Hangzhou Medical College, Hangzhou, Zhejiang Province 310014, China. Email: changxredu@163.com

Abstract

Acute lung injury (ALI) is characterized by severe inflammation and barrier disruption, and effective therapies remain limited. In this study, we investigated nanovesicles derived from the edible fruit *Rosa roxburghii* (RrNVs) in a mouse model of ALI. Oral administration of RrNVs significantly attenuated pulmonary inflammation, immune cell infiltration, edema, and vascular permeability, while preserving endothelial barrier integrity. Network analysis of integrated metabolites and targets revealed citric acid and cyclohexane-related metabolites as central hub nodes in the RrNV-mediated protective network. Furthermore, RrNVs corrected gut microbial

dysbiosis induced by LPS, restored disturbed metabolic pathways including citric acid and cyclohexane metabolism, and reversed aberrant tryptophan-kynurenine turnover, thereby rebalancing gut-lung immune homeostasis. Collectively, these findings demonstrate that fruit-derived nanovesicles, as natural dietary components, exert potent protective effects against ALI through modulation of gut microbiota and tryptophan-related immune metabolism, supporting their potential as a food-based nutritional strategy for inflammatory lung diseases.

Key Words：

Rosa roxburghii extracellular vesicles; acute lung injury; gut–lung axis; tryptophan metabolism; gut microbiota

1. Introduction

Acute lung injury (ALI) is a milder form within the clinical spectrum of acute respiratory distress syndrome (ARDS). It constitutes a life-threatening disorder marked primarily by widespread pulmonary inflammation, disruption of the alveolar-capillary barrier, and refractory hypoxemia. Despite certain advances having been made in supportive care and mechanical ventilation, the mortality rate of ALI/ARDS remains persistently high[1,2]. Current treatment remains primarily supportive, consisting mainly of non-specific anti-inflammatory interventions and symptomatic care, with no approved targeted interventions available[3]. This therapeutic gap highlights the urgent need to develop novel strategies that restore immune homeostasis while minimizing systemic toxicity.

Accumulating studies suggest that the pathogenesis of ALI is not confined to the lungs per se but is closely associated with the gut–lung axis[4,5]. The dysregulation of gut microbiota composition and barrier function can exacerbate lung inflammation through three interrelated mechanisms, namely the translocation of microbial products, alterations in host and microbial metabolic processes, and the migration of gut-derived immune cells[6,7]. Accumulating evidence indicates that gut microbiota dysbiosis can promote the onset and progression of ALI/ARDS, whereas interventions that restore microecological homeostasis or modulate microbiome-derived metabolites alleviate lung injury, highlighting the potential of targeting the gut microbiota in severe respiratory diseases[8]. Among the multiple pathways associated with the microbiome, tryptophan (Trp) metabolism is recognized as a prominent and important factor in regulating mucosal and systemic immunity. Trp undergoes catabolism through the concerted actions of host and microbial enzymes, generating various metabolites including indole derivatives, kynurenines, and 5-hydroxytryptamine (serotonin), which together regulate epithelial barrier integrity, redox balance, and immune cell differentiation[9-11]. Certain metabolites of Trp can promote epithelial repair, support T cell responses, and limit inappropriate inflammatory responses[12]. Notably, gut-derived Trp metabolites can enter the circulatory system and modulate pulmonary immune

status, thereby influencing the onset and progression of lung diseases such as pneumonia and asthma through the gut–Trp–lung axis[13].

At the same time, Plant-derived exosome-like nanovesicles (PNVs) are gaining widespread attention as a novel class of bioactive food-derived particles. These vesicles, composed of a lipid bilayer structure and enriched with various bioactive proteins and nucleic acid molecules, are capable of mediating cross-species communication, exhibit excellent biocompatibility, and are suitable for oral consumption[14]. Accumulating evidence indicates that PNVs derived from edible and medicinal plants can remodel the gut microbiota and regulate inflammation-related signaling pathways. Consequently, nanovesicles isolated from plants such as honeysuckle, ginger, tea, ginseng, and garlic have demonstrated promising beneficial efficacy in the management of inflammatory bowel disease and colitis-associated cancer[15–18]. These findings suggest that PNVs serve as a versatile oral dietary platform capable not only of remodeling the gut microenvironment but also of further regulating distal pulmonary immune responses via the gut–lung axis.

Rosa roxburghii Tratt (RrT) is a nutrient-dense edible fruit traditionally consumed for its digestive and hydrating benefits. Rich in vitamin C, polyphenols, and proanthocyanidins, this fruit has attracted growing interest as a functional food component with potential health-promoting properties. Studies have shown that extracts and polyphenol-rich fractions from *Rosa roxburghii* alleviate dextran sulfate sodium (DSS)-induced colitis by enhancing intestinal tight junctions, reducing oxidative stress, and restoring gut microecological homeostasis [19–22]. Furthermore, proanthocyanidin-rich components of this fruit have been shown to ameliorate liver fibrosis through beneficial remodeling of the gut microbiota [23]. Concurrently, studies have indicated that fermented derivatives of Rosa roxburghii can modulate the oral–gut microbiota axis and exert modulatory effects against bleomycin-induced pulmonary fibrosis[24]. Collectively, these findings support the potential of *Rosa roxburghii* to exert multi-organ regulatory effects through microbiota-dependent mechanisms. However, whether nanovesicles derived from this edible fruit (RrNVs) can alleviate ALI via the

"gut microbiota–tryptophan axis" remains to be further elucidated.

The present study aimed to investigate whether oral administration of RrNVs exerts protective effects on the distal lung tissue in a mouse model of ALI through synergistic remodeling of the gut microbiota and tryptophan metabolism.The results demonstrated that oral administration of RrNVs exerted significant beneficial effects in a lipopolysaccharide (LPS)-induced ALI model, as evidenced by attenuation of pulmonary inflammation, restriction of immune cell infiltration, and amelioration of metabolic disturbances. Mechanistically, RrNVs remodel the gut microbiota and its metabolic profiles, thereby regulating gut–lung immunity, suppressing the overactivation of the tryptophan–kynurenine pathway, and maintaining overall immune homeostasis. Furthermore, integrated metabolite–target network analysis identified citrate, cyclohexane-related metabolites, as well as various terpenoids and aromatic components enriched in RrNVs, which may serve as potential bioactive mediators involved in the regulation of ALI-associated inflammatory signaling, metabolic modulation, and the complement–coagulation pathway.These findings position RrNVs as a food-derived bioactive vesicle population that modulates host nutritional and immune homeostasis via gut microbiota remodeling, offering a mechanistic framework for understanding how dietary fruits confer extra-intestinal health benefits.

2. Experimental Methods

2.1. Preparation and characterization of RrNVs

RrNVs were derived from dried fruits of Rosa roxburghii. The fruits were soaked in phosphate-buffered saline (PBS) and then homogenized using a juicer with the addition of pre-cooled PBS (4 °C). The resulting homogenate was filtered to remove coarse particles and then subjected to multiple cycles of centrifugation at 10,000 rpm and 4 °C using a MX30R high-speed refrigerated centrifuge (RWD Life Science Co., Ltd., Shenzhen, China). After each centrifugation cycle, the supernatant was collected and the pellet was discarded. The combined supernatants were subsequently filtered through

a 200 nm membrane and further purified using a tangential flow filtration system (molecular weight cut-off: 750 kDa; Membrane Solutions (Nantong) Co., Ltd.). The whole process was conducted under low-temperature conditions, and the resultant nanovesicles were sterilized via filtration through a 0.22 μm filter. Morphological characterization was performed using transmission electron microscopy (TEM) and cryo-electron microscopy (Cryo-EM). The samples were fixed with 2% paraformaldehyde and stained with methyl cellulose and uranyl acetate. Observations were performed using Hitachi HT-7700 and FEI Talos F200X transmission electron microscopes, respectively. Particle size distribution and zeta potential were assessed via dynamic light scattering (DLS) on a Malvern Zetasizer Nano ZS-90 and a Nano Coulter counter.

2.2. Stability detection of RrNVs

For assessing the stability of RrNVs under simulated gastrointestinal conditions, 100 μL of RrNVs was combined with 300 μL of either simulated gastric fluid or simulated intestinal fluid, held at 37 °C, and samples were taken at 0.5, 1, 3, 6, 12, and 24 h. At each time point, DLS was used to measure changes in particle size distribution to evaluate their structural stability.

2.3. Nucleic acid analysis

Total RNA was isolated using Trizol reagent (Thermo Fisher Scientific, USA). Use Nano Drop ultra-micro spectrophotometer to determine RNA concentration, and use Bio-Fragment Analyzer to evaluate RNA integrity.

2.4. Lipidomic sequencing analysis

RrNVs were placed in a centrifuge tube containing glass beads, and chloroform: methanol (2:1, v/v) was added for lipid extraction. The samples were subjected to vortex mixing, freeze-thaw cycles, and oscillation treatment, followed by the addition of water to induce phase separation. The organic phase was then collected by centrifugation. After repeated extraction, the combined organic phase is concentrated

and treated, redissolved with isopropyl alcohol, filtered by 0.22 μm filter membrane, and then analyzed by liquid chromatography-mass spectrometry combined technology (LC-MS).

2.5. Proteomic analysis

After extracting the protein, it was verified by SDS-PAGE, and then the enzyme-lyzed peptide segment was analyzed by EASY-nLC 1200 liquid chromatography-tandem mass spectrometry (LC-MS/MS) system (Thermo Fisher Scientific Company of the United States). The screening criteria for differential expression proteins are set to differential multiples > 1.2 (up-up) or < 0.83 (down-down), and $P < 0.05$. Then, the Majorbio cloud platform was used to conduct functional enrichment analysis of Gene Ontology (GO) function entries and Kyoto Encyclopedia of Genes and Genomes (KEGG) signal paths.

2.6. Metabolomic sequencing analysis

RrNVs were added to a centrifuge tube containing glass beads, followed by the addition of a mixed solvent of acetonitrile: methanol: water (2:2:1, v/v/v) for extraction. Following vortexing, freeze-thawing, and grinding, the samples were centrifuged at 12,000 rpm and 4 °C for 10 min. Thereafter, the supernatants were harvested and dried. The dried residue was then reconstituted in an acetonitrile/formic acid solution containing 2-chloro-L-phenylalanine as an internal standard, filtered through a membrane filter, and subsequently analyzed by LC-MS.

2.7. In vivo imaging in mice

In vivo fluorescence imaging was performed at 1, 2, 4, 6, 8, 12, and 24 hours after oral administration of DiR-labeled RrNVs. Imaging was performed using an IVIS Spectrum system (PerkinElmer, USA). At the end of the experiment, the mice were sacrificed, and major organs including the heart, liver, spleen, lungs, kidneys, stomach, small intestine, and colon were collected to measure the fluorescence intensity of each organ.

2.8. Cellular uptake

Inoculate the cells in the confocal culture dish at a density of 1.5×10^5 per dish. The next day, RrNVs with DiO marking were incubated at 37 °C for 0, 12 and 24 hours respectively. After incubation, the cells were washed with PBS three times to remove unbound particles, and then the fluorescence distribution was observed with a laser scanning confocal microscope (Leica SP8).

2.9. LPS-induced ALI model establishment in vivo

Male BALB/c mice were anesthetized with sodium pentobarbital, and then LPS (derived from Escherichia coli O111:B4, 5 mg/kg in 50 μL PBS) was administered via nebulization to establish an ALI model. To evaluate the protective effects, mice were administered with RrNVs once daily for five consecutive days, divided into a low-dose group (10^9 particles/mL) and a high-dose group (10^{10} particles/mL). After LPS treatment, the survival status and behavioral changes of the mice were observed every 4 hours. The mice were euthanized at 24 hours post-modeling, and lung tissues and blood samples were collected for subsequent analysis. All animal experiments were performed following the pertinent guidelines of the Institute of Laboratory Animal Research (ILAR) and received approval from the Animal Ethics Committee of Zhejiang Provincial People's Hospital (Approval No. IACUC-20250624186066).

2.10. Antibiotic administration, FMT, and bacterial colonization

Mice were orally administered a freshly prepared antibiotic cocktail (Abx) consisting of metronidazole (1 g/L), ampicillin (1 g/L), vancomycin (0.5 g/L), and neomycin (1 g/L) for 5 consecutive days. On day 5 after the final administration, fecal samples were collected from the microbiota-depleted mice, homogenized, and inoculated onto Brain Heart Infusion agar supplemented with 10% sheep blood. The samples were subjected to anaerobic culture at 37 °C for 2 days and aerobic culture for 1 day, respectively, to verify whether the gut microbiota had been successfully depleted. For the fecal microbiota transplantation (FMT) experiment, fecal samples (200 mg) from wild-type (WT) mice that had received different treatments (oral administration of PBS or RrNVs)

were added to 1.5 mL of PBS containing sterile silica beads, homogenized at 45 Hz, and then filtered through a 70 μm mesh. Subsequently, 200 μL of the filtered fecal microbiota suspension was administered by oral gavage to antibiotic-pretreated mice.

2.11. Serum Biochemical Analysis and ELISA

Enzyme-linked immunosorbent assay (ELISA) was employed to quantify the concentrations of proinflammatory cytokines IL-1β, IL-6, TNF-α, and the anti-inflammatory cytokine IL-10 in serum collected from mice. The systemic biochemical parameters such as liver transaminases (AST, ALT) and the kidney functioning indicators (BUN, CREA) were also examined to analysis the integrity of multi-organ functioning.

2.12. Quantitative Real-Time PCR

Use Trizol reagent to extract total RNA from lung tissue. After synthesizing complementary DNA (cDNA), SYBR Green PCR premix and genetic-specific primers targeting IL-6, IL-1β, TNF-α and IL-10 are amplified through quantitative polymerase chain reaction (qPCR). Real-time fluorescence quantitative PCR was completed on the ABI 7500 real-time fluorescence quantitative PCR system (Therm Fisher Scientific Company, USA). This method is used to detect the relative expression level of the target transcript.

2.13. Lung W/D Ratio analysis

Pulmonary vascular permeability was assessed by measuring the wet/dry weight ratio (W/D) of lung tissue. After exposing the trachea and esophagus by dissection, the intact lung tissue was removed and weighed to obtain the wet weight. The wet-to-dry (W/D) ratio was then calculated.

2.14. Assessment of pulmonary vascular permeability

To evaluate pulmonary capillary permeability, mice were intravenously injected via the tail vein with 1% Evans blue dye (25 mg/kg, Sigma-Aldrich, USA). Mice were

sacrificed 2 h post-injection, and the right ventricle was perfused with 10 mL PBS to remove residual dye. Lung tissues were collected, blotted dry, and weighed for wet weight. Tissues were placed in formamide (1 mL/100 mg tissue) and incubated at 37 °C for 24 h. After centrifugation at 12,000 rpm for 30 min, the absorbance of the supernatant at 620 nm was measured to assess dye extravasation.

2.15. Analysis of Bronchoalveolar Lavage Fluid (BALF)

Bronchoalveolar lavage fluid (BALF) was obtained from mice at 24 h post LPS induction. BALF was obtained by injecting 1 mL PBS into the trachea followed by repeated gentle aspiration. Immune cell subsets in BALF were analyzed by flow cytometry. Alveolar macrophages were identified by CD11c and Siglec-F, and neutrophils by co-expression of CD11b and Ly6G. Isotype and compensation controls were included.

2.16. Immunofluorescence Staining

Lung sections were incubated with anti-Ly6G and anti-CD3 primary antibodies (eBioscience, Germany), followed by staining with FITC- or TRITC-conjugated secondary antibodies. Also detected were endothelial barrier integrity-related proteins (ZO-1, E-cadherin) and macrophage polarization markers M1 (CD86) and M2 (CD206). Observation and analysis were carried out using a confocal microscope (Leica, Germany).

2.17. 16S rRNA-seq

Following RrNVs intervention, mouse fecal samples were harvested and preserved at −80 °C. Total genomic DNA was isolated via the cetyltrimethylammonium bromide (CTAB) method, and the V3–V4 region of 16S rDNA was subjected to amplification. PCR products were purified, quantified, quality-controlled, and used to construct libraries (concentration ≥ 2 nM). Sequencing data were denoised using the DADA2 algorithm to obtain amplicon sequence variants (ASVs). Alpha and beta diversity analyses were performed based on ASV sequences and abundance tables, and

intergroup differences were assessed by comparing relative species abundances.

2.18. Detection and Analysis of Metabolites in Fecal and Lung Tissues

For Trp metabolite analysis, 50 mg of feces or lung tissue was homogenized using a KZ-II grinder and centrifuged at 12,000 g for 15 min at 4 °C. After the supernatant is filtered by 0.22 μm filter membrane, it is analyzed by gas chromatography-mass spectrometry combined technology (GC-MS) or liquid chromatography-mass spectrometry combined technology (LC-MS).

2.19. Statistical analysis

All statistical analysis is completed using GraphPad Prism software (version 10.0).The data is expressed as mean ± standard deviation (SD). One-way ANOVA or Student's t test is used for inter-group comparison. Taking $P < 0.05$ as the criterion for determining the statistical significance of the difference.

3. Results

3.1. Characterization of RrNVs

Following homogenization, RrNVs were isolated from the supernatant by centrifugation and tangential flow filtration (Fig. 1A). TEM and cryo-EM revealed that RrNVs exhibited a typical bilayer membrane vesicle structure (Fig. 1B). Particles size distribution, mean particle size, and zeta potential were analyzed by DLS. RrNVs carried a negative charge, with a zeta potential of −9.48 mV and a size range of 54–146 nm (Fig. 1C-D). Further measured by Nano Coulter counter, the mean particle size was 75.0 ± 18.7 nm, and the particle concentration was 4.31×10^{12} particles/mL (Fig. 1F). The nucleic acids isolated from RrNVs ranged from 20 to 1,183 nt in length, with the majority concentrated in the 20–200 nt range (Fig. 1F). Protein quantification in RrNVs is shown in Fig. 1G. Stability of RrNVs in simulated gastrointestinal environments, with PBS as a control. Morphological and particle size analyses showed that RrNVs largely maintained structural integrity under simulated gastrointestinal conditions, exhibiting good tolerance to acidic environments and enzymatic degradation,

supporting their potential application as oral nano-delivery vehicles (Fig. 1H).

The molecular composition of RrNVs was systematically characterized by integrated multi-omics analysis. Lipidomics analysis (Fig. S1A–B) revealed significant heterogeneity among lipid subclasses, with the major lipid types including phosphatidylethanolamine (PE), phosphatidylcholine (PC), monohexosyl ceramide (Hex1Cer), and cardiolipin (CL). Proteomics analysis (Fig. S1C) identified multiple functional proteins, including stress-related heat shock proteins, metabolic enzymes, and cytoskeleton-associated proteins. KEGG pathway enrichment analysis indicated that these differential proteins were mainly involved in biological processes such as cellular metabolism, signal transduction, and environmental adaptation (Fig. S1D). Metabolomics analysis (Fig. S1E) revealed that most identified metabolites were lipids or lipid-related molecules. KEGG enrichment analysis of the top 20 pathways (Fig. S1F) further indicated significant alterations in pathways including amino acid metabolism, lipid metabolism, and energy metabolism.

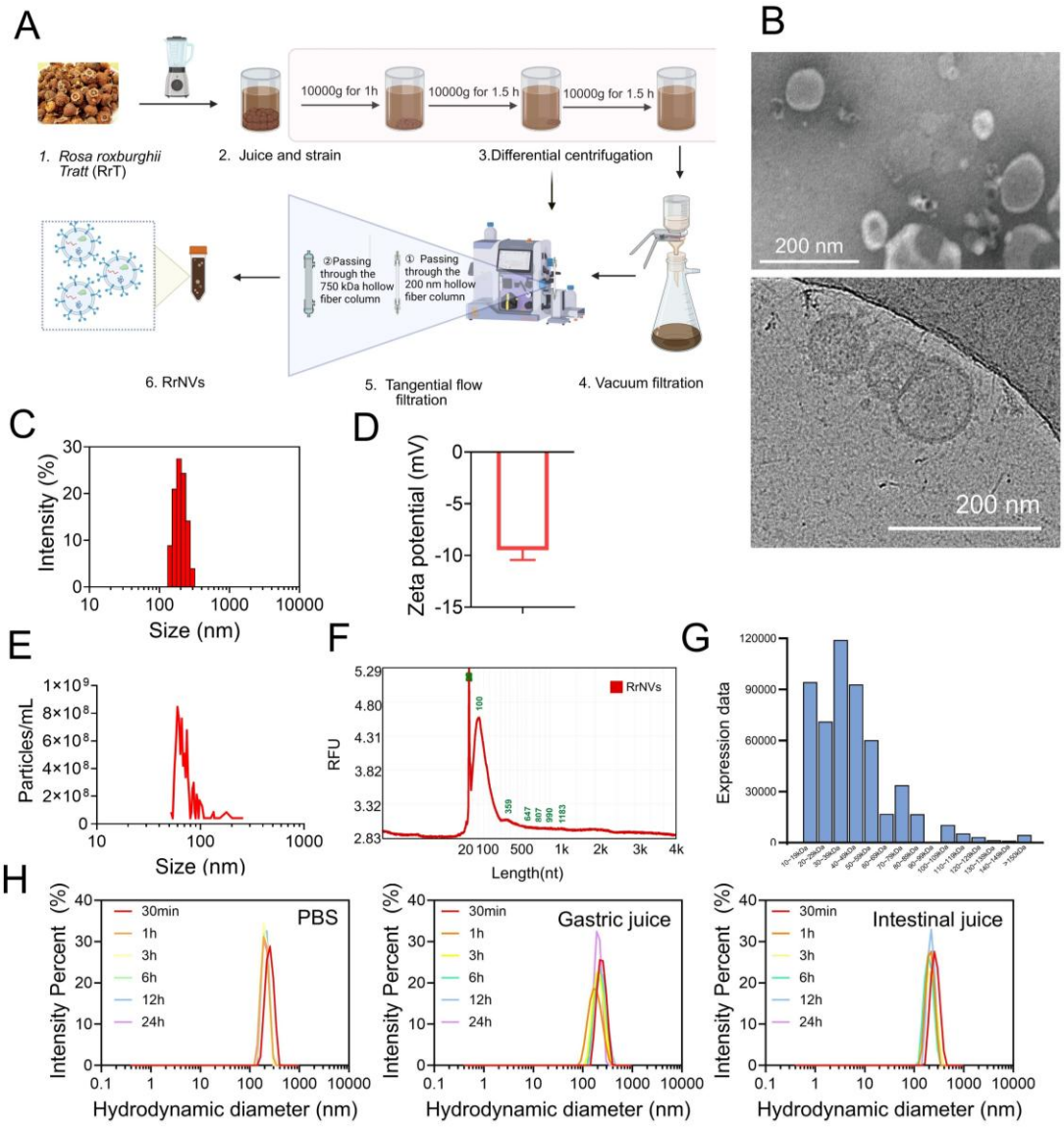

Fig. 1. Identification and characterization of RrNVs. (A) RrNVs were isolated and purified according to a detailed and standardized protocol. (B) Visualization of RrNVs by TEM (upper panel) and Cryo-TEM (lower panel). (C–D) DLS-based assessment of RrNVs, showing (C) their zeta potential and (D) their size distribution profiles. (E) Counting of RrNVs particles. (F) RNA of RrNVs were separated according to size using the Bio-Fragment Analyzer. (G) The protein size and content of RrNVs. (H) Changes in size distribution of RrNVs after incubation with PBS, gastric juice and intestinal juice at 37°C. Scale bar = 200 nm.

3.2. Protective efficacy of RrNVs in LPS-induced ALI mouse model

The experimental design is shown in Fig. 2A. H&E staining showed that LPS

treatment successfully induced ALI, characterized by alveolar structural disruption and pulmonary congestion.High-dose RrNVs (RrNVs-H) significantly alleviated these pathological injuries (Fig. 2D) and reduced lung injury scores (Fig. 2B), indicating a protective effect of RrNVs against LPS-induced ALI. Pulmonary edema was assessed by the wet/dry weight ratio (W/D). High-dose RrNVs significantly reduced pulmonary edema (Fig. 2C). Serum cytokine analysis showed that LPS stimulation significantly elevated pro-inflammatory cytokines IL-1β, IL-6, and TNF-α, whereas oral RrNVs markedly suppressed these inflammatory factors and increased anti-inflammatory IL-10 levels (Fig. 2G). Based on the above results, the high-dose RrNVs group was selected for subsequent experiments**.**

Pulmonary vascular integrity was further assessed by i.v. injection of EBA.Compared with the LPS group, RrNVs treatment significantly reduced Evans blue extravasation, restored vascular barrier function, and decreased LPS-induced vascular hyperpermeability (Fig. 2E–F). RT-qPCR analysis of lung tissue showed that RrNVs significantly reduced the expression of pro-inflammatory cytokines (IL-1β, IL-6, TNF-α) while upregulating the expression of the anti-inflammatory cytokine IL-10. RrNVs treatment also alleviated oxidative stress, as evidenced by decreased expression of inducible nitric oxide synthase (iNOS) (Fig. 2H). Since iNOS is a classic marker of M1 macrophage polarization, one mechanism by which RrNVs alleviate ALI may involve inhibiting M1 macrophage activation. To further characterize the dynamic changes of inflammatory cells during ALI, BALF was collected and analyzed by flow cytometry. RrNVs treatment significantly reduced neutrophil infiltration and increased the number of alveolar macrophages (Fig. 2I, J). Our data suggest that RrNVs likely alleviate pulmonary inflammation by inhibiting inflammatory cell recruitment into the alveoli and restoring protective alveolar cells.

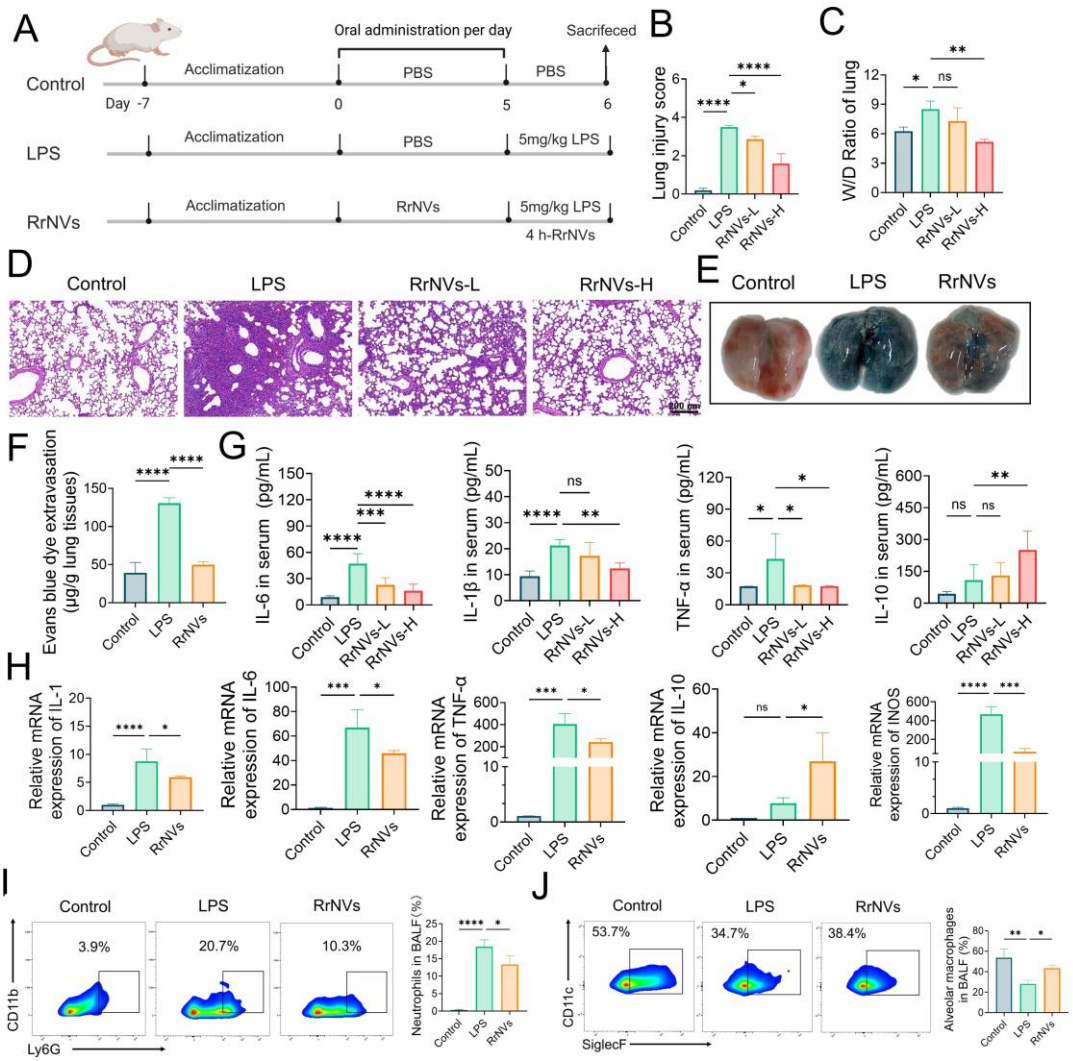

Fig. 2. The therapeutic effects of RrNVs *in vivo*. (A) Schematic illustration depicts the establishment of the LPS-induced ALI model. (B) Injury score of lung tissue. (C) Wet/Dry weight ratio of lung tissues in experimental groups. (D) Histological analysis (H&E) and, showcasing the protective effects of RrNVs at a microscopic level (scale bar, 200 μm). (E-F) Evans Blue extravasation in lung tissues(E) and statistical analysis(F). (G) The changes of inflammatory factors in serum. (H) The changes of inflammatory factors lung tissue. (I-J) The changes of neutrophils and alveolar macrophages in BALF of mice. Data are presented as mean ± SD (n=5) (***$p < 0.001$, **$p < 0.01$, *$p < 0.05$, ns: not significant)

3.3. Network pharmacology reveals the key active components and therapeutic mechanisms of RrNVs in ALI.

To elucidate the protective mechanism of RrNVs, their chemical composition was first systematically characterized, followed by network pharmacology analysis to screen for potential active ingredients and associated pathways in ALI.

The identified compounds covered multiple chemical categories, including terpenoids, indoles, flavonoids, tannins, and phenolic acids, as well as a certain number of unclassified compounds (Fig. 3A). Gene Ontology (GO) enrichment analysis indicated that the targets of RrNVs were mainly enriched in key biological processes during ALI pathogenesis, including coagulation, hemostasis, inflammatory response, and tissue repair (Fig. 3B). KEGG pathway enrichment analysis showed that RrNVs targets were significantly enriched in complement and coagulation cascades, infection-related pathways, and inflammatory and immune regulatory pathways (Fig. 3C). These pathways are closely associated with the core pathological features of ALI, suggesting that the protective effects of RrNVs may be exerted synergistically through multiple mechanisms.

In the protein-protein interaction (PPI) network, the targets of RrNVs were mainly concentrated on hub nodes regulating key processes of ALI pathogenesis, including inflammatory signal amplification, immune activation, and cell death (Fig. 3D). Further analysis identified TNF, IL6, CASP3, TLR4, and PTGS2 as core hub genes (Fig. 3D), suggesting their potential roles in regulating key pathological signaling pathways in ALI. Concurrent compound–target–disease network analysis indicated that terpenoids and aromatic derivatives enriched in RrNVs, including farnesol, nerolidol, carvacrol, farnesyl acetone, camphor, and safrole, possess anti-inflammatory, antioxidant, and anti-apoptotic biological activities. These components can interact with various inflammation-related genes, including TNF, IL6, IL1B, PTGS2, NOS2, HMOX1, VEGFA, ICAM1, CASP3, and CASP8, thus constructing a multi-target regulatory network associated with ALI (Fig. 3E).

Additionally, component–target–pathway–ALI network analysis further identified citrate and cyclohexane-related metabolites as core active metabolites in RrNVs (Fig. 3F). These molecules regulate multiple key ALI-related targets, including complement

component C3, coagulation factor II (F2), and tissue factor (F3), thereby affecting KEGG pathways involved in complement activation, coagulation cascade, and inflammatory immune responses. Through this convergent regulatory network, RrNVs exert multi-dimensional protective effects in ALI.

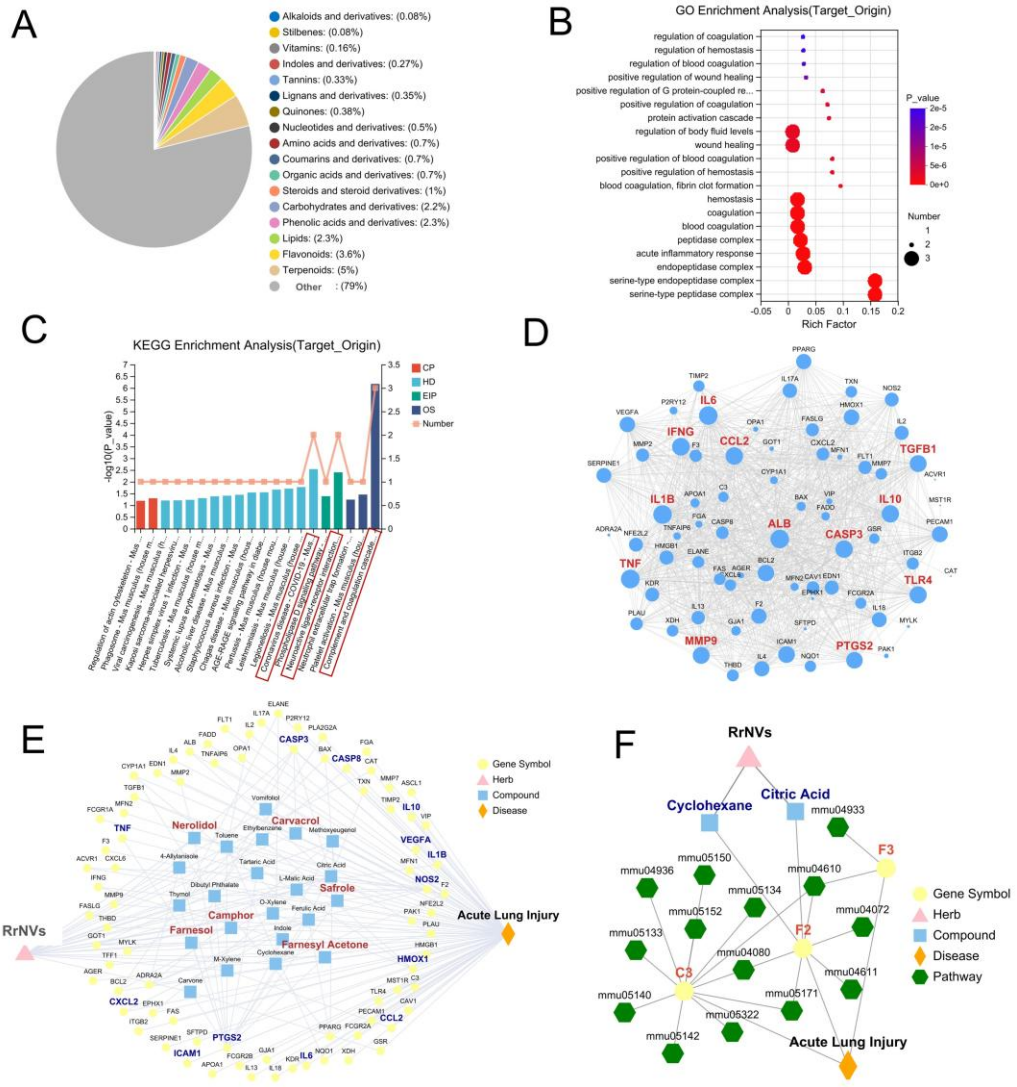

Fig. 3. Network pharmacology reveals the key active components and therapeutic mechanisms of RrNVs in ALI. (A) Chemical classification of RrNVs-derived constituents. (B) GO enrichment analysis of the predicted targets of RrNVs. (C) KEGG pathway enrichment analysis. (D) Protein–protein interaction (PPI) network constructed from RrNVs targets. (E) Compound–target–disease interaction network. (F) Herb–component–target–disease–pathway network showing metabolite-mediated regulation of key targets.

3.4. Distribution of RrNVs in vivo and in vitro

To evaluate the in vivo biodistribution of orally administered RrNVs, an ALI mouse model was established by intratracheal nebulization of LPS (5 mg/kg). Mice were randomly divided into three groups: healthy control group, LPS-induced ALI model group (LPS, 5 mg/kg), and RrNVs-treated group (RrNVs + LPS, 5 mg/kg LPS). After LPS induction, DiR-labeled RrNVs (0.3 mg/mL) were orally administered to mice. Biodistribution of RrNVs was dynamically monitored by whole-body fluorescence imaging at 0, 1, 2, 4, 6, 8, 12, and 24 h after oral gavage. Fluorescence signal peaked at 4–8 h post-administration, gradually declined, but remained weakly detectable at 24 h (Fig. 4A). IVIS imaging revealed distinct tissue distribution characteristics, with fluorescence accumulation in the intestine reaching a maximum at 4 h (Fig. 4B), whereas lung signals were observed only in the RrNVs-treated group and peaked at 4–8 h (Fig. 4C). The RrNVs-treated group showed significantly increased fluorescence intensity in lung tissue and prolonged retention time, indicating strong lung tissue targeting properties.

To determine whether RrNVs can be taken up by cells, their cellular uptake was examined in alveolar macrophage cell lines (RAW 264.7 and MH-S) under LPS-stimulated conditions (Fig. 4D–E). The results showed that under inflammatory conditions, RrNVs were efficiently taken up by both macrophage cell lines for up to 24 h, positioning them as a promising strategy for targeting inflammatory lung diseases.

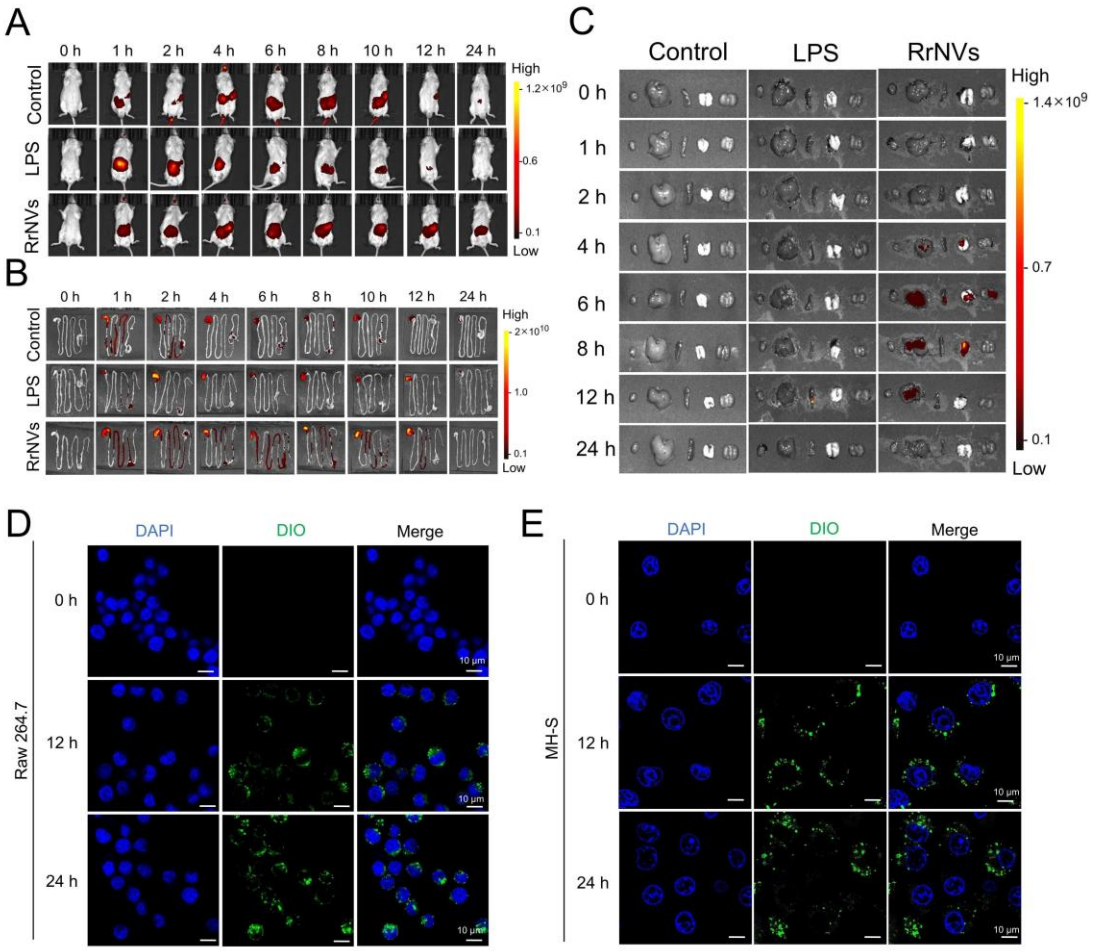

Fig. 4. RrNVs distribution in vivo and in vitro. (A) Whole body imaging of mice at 0, 1, 2, 4, 6, 8, 12 and 24 h after oral administration of RrNVs. (B-C) The distribution of DIR-labeled RrNVs in the intestine (B) and the main organs of mice (C) at different time points. (D-E) Fluorescence detection of RrNVs uptake by Raw 264.7 and MH-S cells (scale bar, 10 μm). Data are presented as mean ± SD (n=3) (***$p < 0.001$, **$p < 0.01$, *$p < 0.05$, ns: not significant)

3.5. *RrNVs attenuate LPS-induced pulmonary inflammation and restore epithelial and macrophage homeostasis.*

To evaluate immune cell infiltration in the lung parenchyma, immunocolocalization was performed on lung tissues from the control, LPS, and RrNVs-treated groups. Results showed that LPS stimulation significantly induced infiltration of $Ly6G^+$ neutrophils and $CD3^+$ T cells, whereas RrNVs treatment markedly reduced the accumulation of both immune cell types (Fig. 5A). Furthermore, RrNVs protected lung

epithelial integrity. LPS significantly disrupted tight junction protein ZO-1 and adherens junction protein E-cadherin, whereas RrNVs treatment restored a continuous and enhanced fluorescence signal at cell junctions, indicating epithelial barrier recovery (Fig. 5B). As shown in Fig. 5C, RrNVs regulated macrophage polarization, as evidenced by downregulation of the M1 marker CD86 and upregulation of the M2 marker CD206, suggesting that they promote macrophage conversion to a reparative phenotype. RrNVs exert protective effects against LPS-induced lung injury by inhibiting pro-inflammatory immune cell recruitment, maintaining epithelial barrier integrity, and remodeling macrophage polarization status.

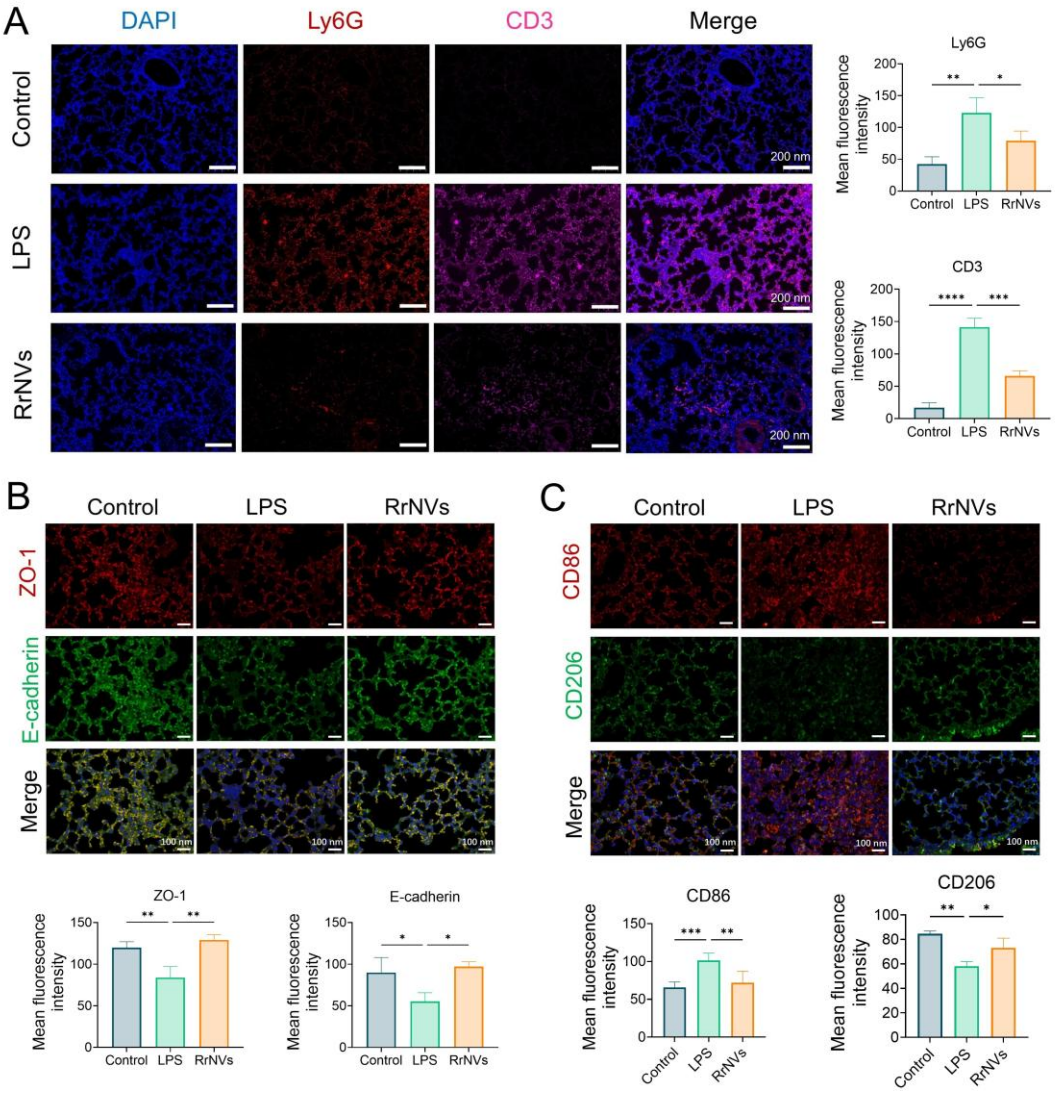

Fig. 5. RrNVs attenuate LPS-induced pulmonary inflammation and restore

epithelial and macrophage homeostasis. (A) Immunofluorescence staining of lung sections showing neutrophils (Ly6G, red) and T cells (CD3, pink). Scale bars, 200 μm. (B) Representative images of tight junction protein ZO-1 (red) and epithelial marker E-cadherin (green) in lung tissues. (Scale bars, 100 μm). (C) Immunofluorescence staining of M1 macrophage marker CD86 (red) and M2 macrophage marker CD206 (green). Scale bars, 100 μm. Data are presented as mean ± SD (n=5) (***$p < 0.001$, **$p < 0.01$, *$p < 0.05$, ns: not significant)

3.6. RrNVs restore gut microbial diversity and composition disrupted by LPS exposure.

To investigate the effect of RrNVs on gut microbiota diversity, 16S rRNA sequencing analysis was performed. Rarefaction analysis revealed that the sequencing depth and coverage were adequate (Fig. 6A). Alpha diversity analysis showed that LPS stimulation significantly reduced gut microbiota richness, whereas RrNVs treatment effectively restored overall diversity (Fig. 6B). Principal coordinates analysis (PCoA) based on amplicon sequence variants (ASVs) revealed distinct clustering patterns among the three groups, indicating that RrNVs reshaped the microbiota structure to near-normal status after LPS-induced dysbiosis (Fig. 6C). At the phylum level, LPS treatment significantly increased the Firmicutes/Bacteroidetes (F/B) ratio, a typical marker of dysbiosis. After RrNVs intervention, this ratio was restored to a relatively balanced state (Fig. 6D). Community structure analysis and heatmap results (Fig. 6E–G) showed that LPS treatment promoted the enrichment of pro-inflammatory-associated microbiota while reducing the abundance of beneficial bacteria. RrNVs treatment reversed these changes, thereby restoring gut microecological homeostasis. RrNVs effectively ameliorated LPS-induced gut microbiota dysbiosis by restoring microbial diversity, reestablishing the ratio of dominant flora, and modulating the abundance of inflammation-associated microbiota.

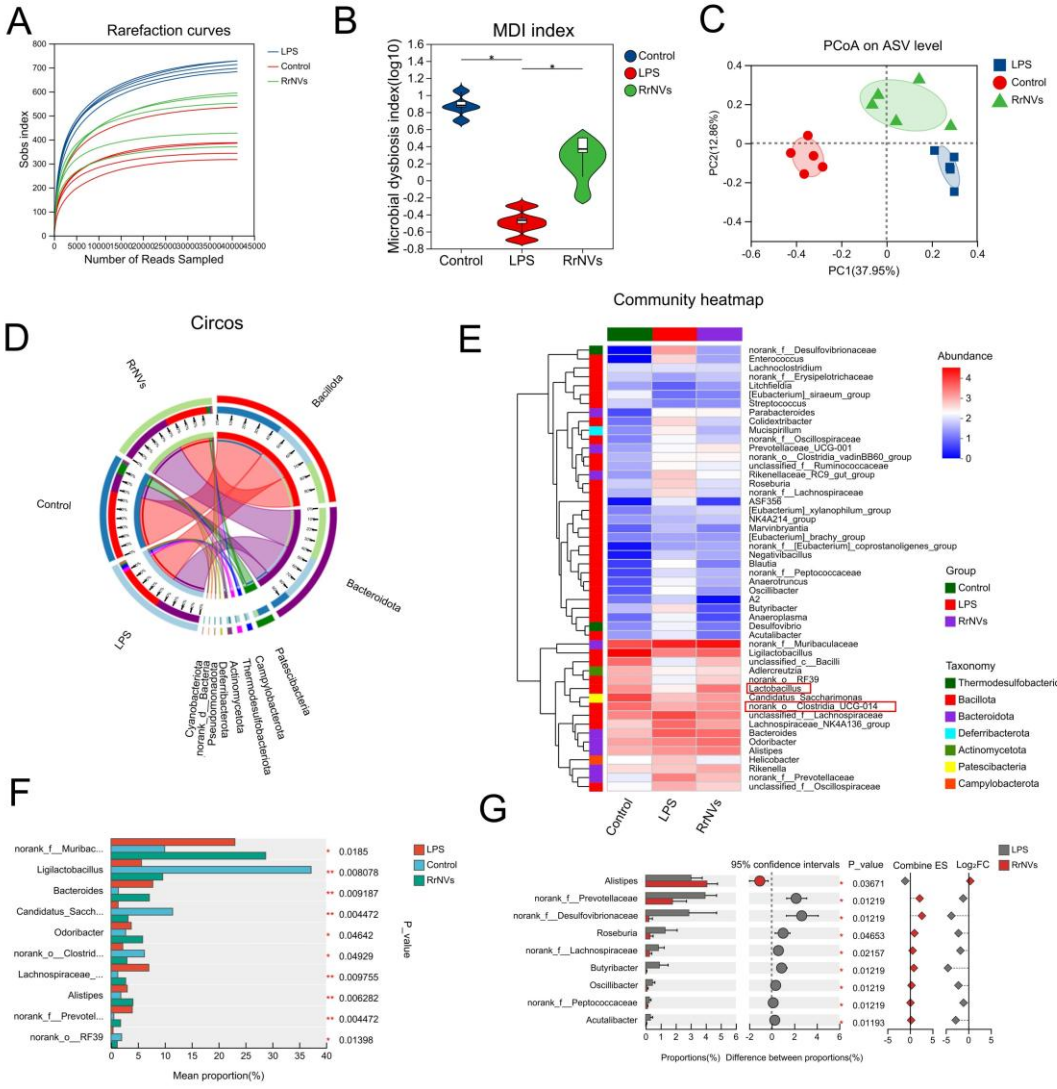

Fig. 6. RrNVs restore gut microbial diversity and composition disrupted by LPS exposure. (A) Rarefaction curves showing sequencing depth and species richness across groups. (B) Microbial diversity index (MDI) analysis. (C) Principal coordinate analysis (PCoA). (D) Circos plot visualizing microbial taxonomic relationships and relative abundances. (E) Community heatmap displaying relative abundance of dominant genera across samples. (F) The mean proportion of significantly changed bacterial genera. (G) Wilcoxon rank-sum test identifying specific taxa with significant differences at the genus level. Data are presented as mean ± SD (n=5) (***$p < 0.001$, **$p < 0.01$, *$p < 0.05$, ns: not significant)

3.7. RrNVs alleviate ALI by regulating immune homeostasis along the gut–lung axis.

To further explore the relationship between gut microbiota changes and distal lung

outcomes, integrated multi-omics analysis was performed, focusing on key taxa identified in Fig. 6E, particularly *Lactobacillus* and *Clostridia*. It has been established that their interaction is a key factor in regulating intestinal tryptophan metabolism. Disruption of this interaction directly leads to dysregulation of the intestinal tryptophan metabolic pathway, which in turn may transmit metabolic abnormality signals to the lungs via the gut-lung axis, thereby influencing distal lung outcomes. Based on the above scientific rationale and the key bacterial taxa identified in this study, we first focused on the interaction between these two groups, and subsequently performed targeted sequencing of tryptophan metabolism in both intestinal and lung tissues to systematically detect relevant indicators within the tryptophan metabolic pathway.

Tryptophan metabolomics analysis was performed on fecal samples from mice in the control, LPS, and RrNVs-treated groups. PCA revealed clear separation among the three groups, and RrNVs ameliorated LPS-induced diversity changes (Fig. 7A). Targeted analysis of tryptophan metabolism showed that LPS induction caused significant metabolic disturbances (Fig. 7B), characterized by marked reductions in indole pathway- and nicotinamide pathway-related metabolites, which were largely restored by RrNVs treatment. Heatmap analysis further confirmed that LPS generally suppressed the production of indole derivatives, whereas RrNVs promoted the restoration of these metabolic processes to normal levels (Fig. 7C). Quantitative analysis of individual metabolites (Fig. 7D) showed that LPS treatment significantly altered the levels of nicotinic acid, quinolinic acid, and tryptophan. RrNVs intervention markedly ameliorated these changes, elevated nicotinamide and 5-hydroxyindoleacetic acid levels, and further restored L-tryptophan, indole-3-acetic acid, and indole-3-ethanol. Furthermore, RrNVs inhibited the accumulation of harmful metabolites (e.g., quinolinic acid) induced by LPS.

Targeted metabolomics analysis of tryptophan metabolites was performed in lung tissue. PCA similarly showed clear metabolic separation among the three groups (Fig. 8A). LPS induction caused widespread disruption of multiple tryptophan metabolic pathways, whereas RrNVs treatment largely restored these changes (Fig. 8B). Heatmap

analysis showed that LPS significantly suppressed metabolites in the indole, kynurenine, and nicotinamide pathways, whereas RrNVs treatment restored these metabolite levels to near the control group (Fig. 8C). Statistical analysis showed that LPS significantly elevated the levels of kynurenine, quinolinic acid, xanthurenic acid, nicotinic acid, and nicotinamide. Notably, RrNVs effectively ameliorated these changes and restored metabolic balance in the kynurenine and nicotinamide pathways (Fig. 8D). RrNVs treatment also inhibited the spread of inflammatory signals in lung tissue and prevented the aberrant shunting of tryptophan to the kynurenine pathway. These data indicate that RrNVs effectively ameliorate LPS-induced tryptophan metabolic disturbances in lung tissue.

To explore how RrNVs coordinately regulate gut microbiota, tryptophan metabolism, and pulmonary inflammation, integrated analysis was performed on 16S rRNA sequencing data and tryptophan metabolic profiles from intestinal and lung tissues. Results showed significant correlations between fecal tryptophan metabolites and gut microbiota (Fig. S2A). Pro-inflammatory bacterial groups (e.g., *Bacteroides* and *Enterococcus*) were negatively correlated with anti-inflammatory indole metabolites, whereas butyrate-producing taxa (e.g., *Muribaculaceae* and *Ruminococcaceae*) showed positive correlations. Similarly, tryptophan metabolites in lung tissue were also strongly correlated with gut microbiota composition (Fig. S2B): *Ruminococcaceae* and *Ruminococcus* were positively correlated with anti-inflammatory indole derivatives, whereas *Enterococcus* and *Bacteroides* showed negative correlations.

Our data demonstrate that RrNVs synergistically regulate the “gut–tryptophan–lung” immune axis by remodeling the gut microbiota and promoting the generation of beneficial tryptophan metabolites. Interestingly, RrNVs also restored the metabolic balance of the tryptophan–kynurenine pathway in lung tissue, which may depend on gut microbiota remodeling and enhanced conversion of tryptophan toward anti-inflammatory metabolites. This mechanism helps suppress pulmonary inflammation and achieves bidirectional immune regulation along the gut–lung axis.

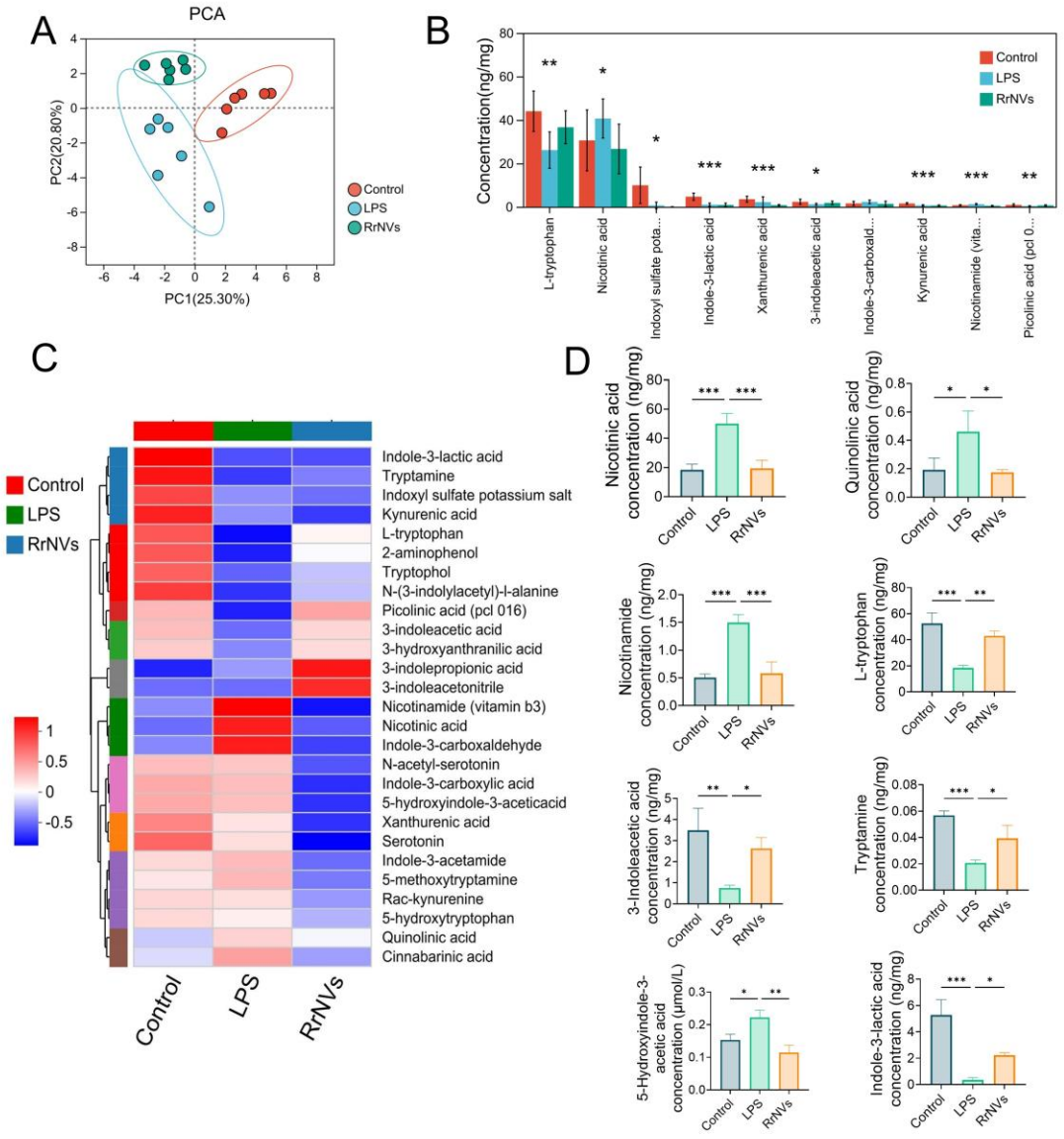

548

549 **Fig. 7. RrNVs can restore gut tryptophan metabolites disrupted by LPS.** (A)
550 Principal Component Analysis (PCA). (B) Quantification of Key Tryptophan
551 Metabolites. (C) Heatmap of Tryptophan Metabolism Profiles Across Experimental
552 Groups. (D) Statistical Analysis of Metabolite Levels. Data are presented as mean ± SD
553 (n=5) (***$p < 0.001$, **$p < 0.01$, *$p < 0.05$, ns: not significant)

554

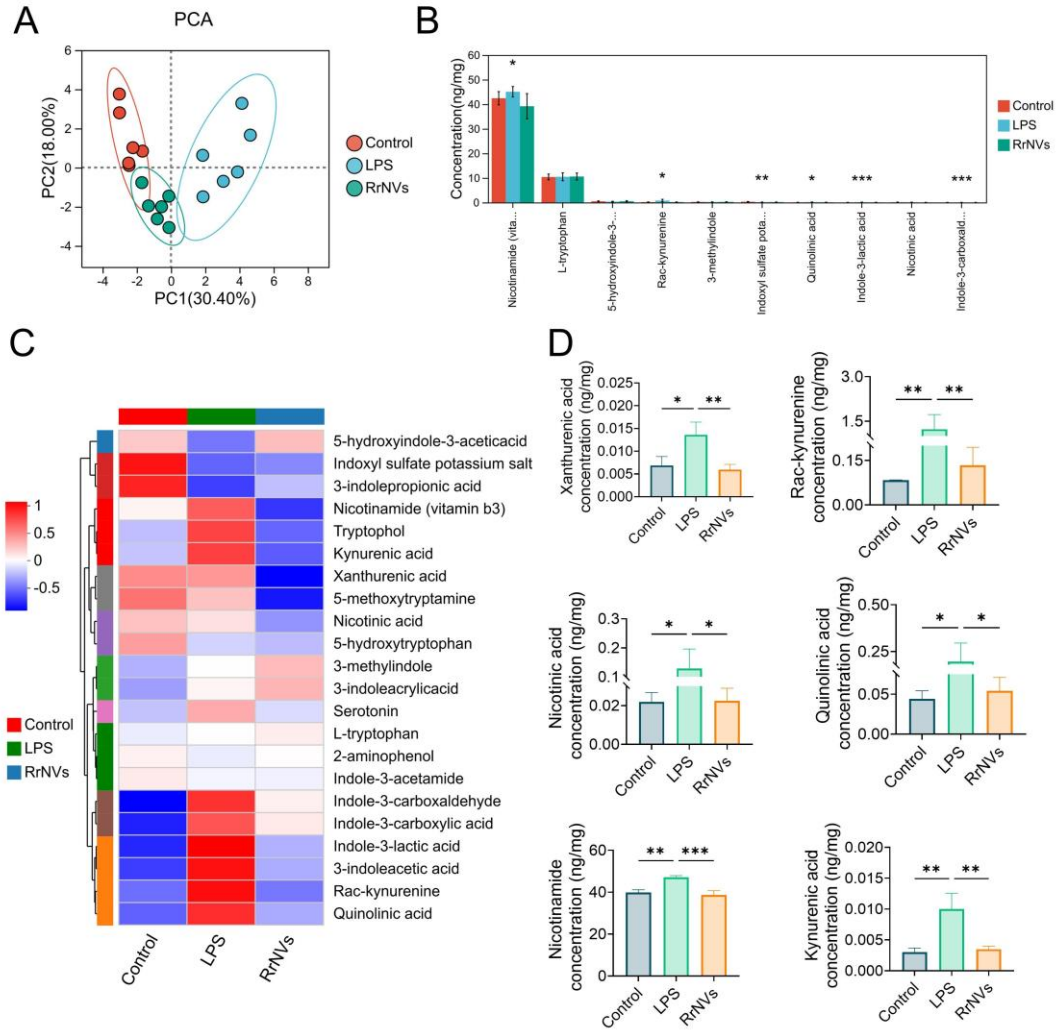

Fig. 8. RrNVs restore lung tryptophan metabolites disrupted by LPS. (A) Principal Component Analysis (PCA). (B) Quantification of Key Tryptophan Metabolites. (C) Heatmap of Tryptophan Metabolism Profiles Across Experimental Groups. (D) Statistical Analysis of Metabolite Levels. Data are presented as mean ± SD (n=6) (***p < 0.001, **p <0.01, *p <0.05, ns: not significant)

3.8. RrNVs protect against LPS-induced ALI in antibiotic-treated, microbiota-depleted mice.

To evaluate the effects of RrNVs on intestinal homeostasis and lung injury independent of the original gut microbiota, a broad-spectrum antibiotic cocktail containing neomycin, vancomycin, metronidazole, and ampicillin was used to deplete the commensal microbiota, thereby establishing a microbiota-depleted mouse model (Fig. 9A). Results showed that LPS induced significant body weight loss in mice, and

RrNVs treatment failed to alleviate this change (Fig. 9B). Compared with the control group, LPS treatment significantly increased lung injury scores in mice, whereas RrNVs exhibited only mild histological protection under microbiota-depleted conditions (Fig. 9C–D). Further serum cytokine analysis showed that RrNVs treatment only modestly reduced systemic IL-6 levels, with no significant effect on IL-1β, TNF-α, or IL-10 (Fig. 9E). Therefore, in the absence of intact gut microbiota, the protective effect of RrNVs against LPS-induced ALI was markedly attenuated.

Fecal microbiota transplantation (FMT) experiments further confirmed that the protective effect of RrNVs is dependent on the gut microbiota. After microbiota depletion, fecal microbiota from untreated donors (FMT-C) or from RrNVs-treated donors (FMT-R) was transplanted into recipient mice (Fig. 9F). After LPS induction, mice receiving FMT-C exhibited significant body weight loss, whereas those receiving FMT-R showed markedly improved recovery (Fig. 9G). Furthermore, mice receiving FMT-R exhibited significantly reduced lung injury scores after LPS induction, with marked alleviation of alveolar structural disruption and inflammatory cell infiltration (Fig. 9H–I). Serum cytokine analysis showed that the RrNVs-remodeled gut microbiota significantly reduced IL-6, IL-1β, and TNF-α levels, while partially restoring IL-10 levels (Fig. 9J).

When administered alone, RrNVs only slightly downregulated some inflammatory factors, but showed limited improvement in global pulmonary inflammation. In contrast, the RrNVs-remodeled gut microbiota significantly enhanced its protective effects on the lungs, effectively alleviating alveolar inflammation and reducing pro-inflammatory cytokine secretion. Based on the gut microbiota, the inhibitory effect of RrNVs on pulmonary inflammation is further amplified. Thus, RrNVs-mediated gut microbiota remodeling plays a key role in suppressing systemic inflammation and reversing ALI.

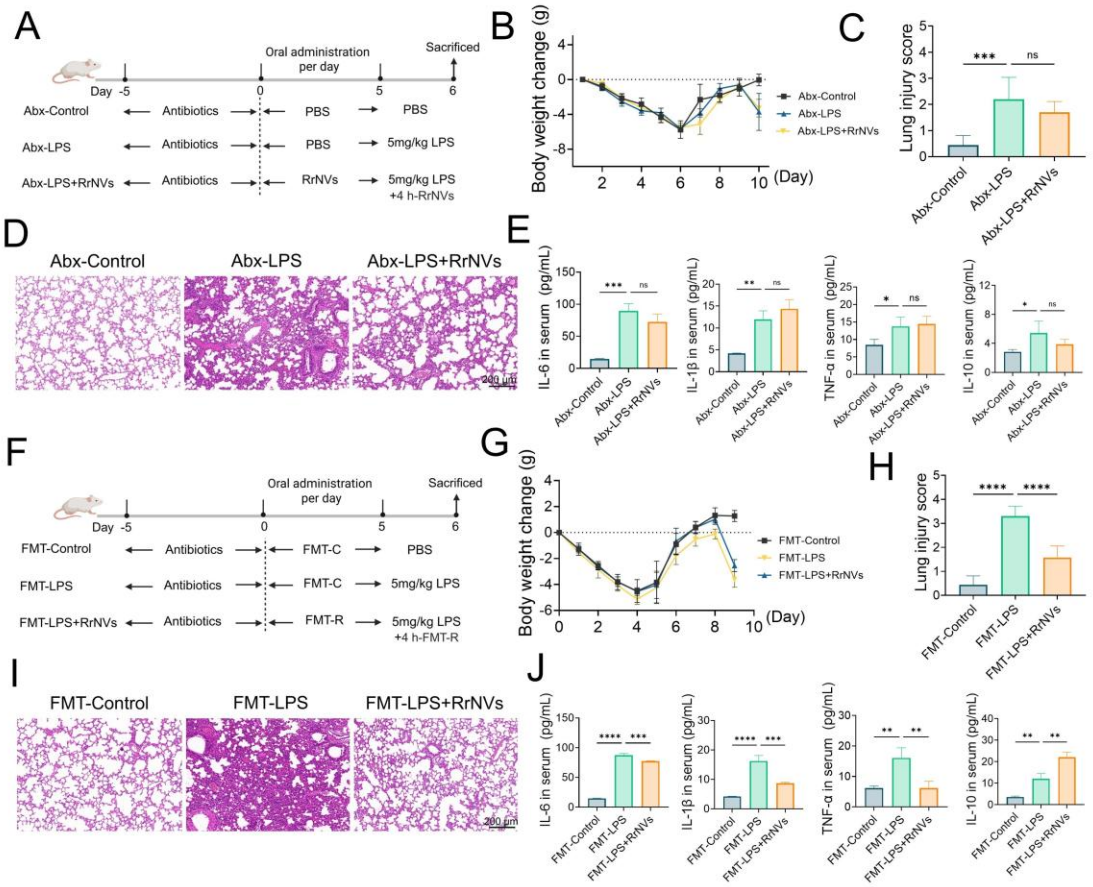

Fig. 9. Effects of RrNVs treatment on LPS-induced experimental ALI symptoms in BALB/c mice with depleted gut microbiota. (A) Schematic depiction of the LPS-induced pseudo-germ-free mouse model of ALI. (B) Alterations in body weight across a 10-day period. (C) Microscopic histological evaluation using hematoxylin and eosin staining (scale bar, 200 μm). (D) Lung tissue injury score. (E) Alterations in serum inflammatory factor levels. (F) Schematic representation of the LPS-induced FMT ALI model. (G) Body weight alterations over a 10-day span. (H) Microscopic histological assessment via hematoxylin and eosin staining (scale bar, 200 μm). (I) Lung tissue injury scoring. (J) Serum inflammatory factor changes. Data are presented as mean ± SD (n=5) (***$p < 0.001$, **$p < 0.01$, *$p < 0.05$, ns: not significant)

3.9. Biosafety Evaluation of RrNVs

The therapeutic effects of RrNVs are partly attributed to their targeting of inflammatory lesions and low toxicity.To evaluate its in vivo biosafety, healthy BALB/c mice were orally administered a high dose of RrNVs daily for 8 consecutive days.

Throughout the treatment period, no significant difference in body weight change was observed between mice treated with RrNVs and the PBS control group (Fig. S3B), and no abnormal body weight loss occurred. Routine serum biochemical analysis showed that key liver and kidney function indicators, including BUN, CRE, ALT, and AST, were within normal physiological ranges, with no significant differences among groups, indicating that RrNVs did not cause obvious hepatotoxicity or nephrotoxicity (Fig. S3C–D). Histopathological analysis showed that, compared with the control group, the RrNVs-treated group exhibited no obvious pathological damage or inflammatory lesions in major organs (heart, liver, spleen, lungs, and kidneys) (Fig. S3A).

In vitro, macrophages incubated with various concentrations of RrNVs for 24 h showed cell viability >85% at all tested concentrations, with no obvious cytotoxicity (Fig. S3E–F). Furthermore, the hemolysis assay showed that RrNVs exhibited low hemolytic activity, indicating good hemocompatibility (Fig. S3G). RrNVs exhibited favorable biosafety both in vitro and in vivo.

4. Discussion

In recent years, PNVs have garnered considerable attention as orally deliverable food-derived bioactive particles capable of crossing biological barriers and modulating inflammatory responses, metabolic processes, and tissue homeostasis[25,26]. Given that components of Rosa roxburghii fruits have been shown to exert pulmonary protection via microbiota-related mechanisms[27]. Our study shows that RrNVs significantly alleviate LPS-induced ALI in a manner partially dependent on the gut microbiota. Oral administration of RrNVs suppresses systemic and pulmonary pro-inflammatory cytokine production, limits recruitment of inflammatory immune cells, promotes macrophage polarization toward an M2-like phenotype, and remodels immunometabolism of the tryptophan–kynurenine pathway, thereby restoring pulmonary vascular endothelial barrier integrity.

Within the framework of the gut–lung axis, ALI is characterized by an excessive

637 inflammatory response, accompanied by neutrophil infiltration, epithelial injury, and
638 systemic cytokine dysregulation. Overproduction of pro-inflammatory cytokines such
639 as IL-6, IL-1β, and TNF-α, along with uncontrolled activation of the innate immune
640 system, can trigger a cytokine storm-like response, thereby rapidly amplifying tissue
641 damage[28]. Our results are consistent with this model: LPS stimulation significantly
642 elevated circulating pro-inflammatory cytokine levels and caused severe
643 histopathological damage, whereas RrNVs intervention markedly suppressed these
644 cytokines, reduced lung injury scores, and attenuated pulmonary edema and increased
645 vascular permeability. These results suggest that RrNVs interrupt the feed-forward
646 amplification loop of inflammation by suppressing macrophage activation and limiting
647 neutrophil recruitment. Macrophage-mediated inflammation is a key determinant of
648 ALI progression, with persistent M1 polarization exacerbating tissue damage, whereas
649 M2 polarization promotes inflammation resolution and tissue repair[29,30]. RrNVs
650 promoted macrophage polarization toward an M2-like phenotype, consistent with
651 recent studies showing that food-derived vesicles and microbial metabolites ameliorate
652 ALI by modulating macrophage phenotype[31,32].

653 Furthermore, network pharmacology and PPI analysis further identified TNF, IL6,
654 CASP3, TLR4, and PTGS2 as key hub nodes of RrNVs action, supporting their multi-
655 target immunomodulatory mechanism. Consistent with the above immunomodulatory
656 findings, the integrated metabolite–target network analysis further identified citrate and
657 cyclohexane-related metabolites as core nodes in the RrNVs protective network.
658 Citrate-related metabolic processes have been shown to regulate mitochondrial function
659 and immune responses under inflammatory stress[33–35]. Concurrently, the synergistic
660 regulation of complement component C3, coagulation factor II (F2), and tissue factor
661 (F3)—all important ALI-related targets—suggests that RrNVs may act by modulating
662 complement activation and coagulation dysfunction, both recognized as key drivers of
663 ARDS pathogenesis[36]. Collectively, these data support a convergent protection model
664 in which RrNVs exert protective effects by synergistically regulating multiple pathways,
665 including inflammatory amplification, the complement–coagulation cascade, and

innate immune activation. Additionally, terpenoids and aromatic compounds enriched in RrNVs, such as farnesol, nerolidol, carvone, and farnesyl acetone, have been reported to exert anti-inflammatory and antioxidant activities in lung, intestinal, and metabolic inflammation models[37–40]. The interaction of these components with the ALI-related gene network further supports that RrNVs, as naturally derived food vesicles, possess multi-component, multi-target, and multi-pathway bioactive characteristics.

In addition to direct immunomodulation, alterations in the gut–lung axis are also important factors affecting pulmonary inflammation. Gut microbiota dysbiosis exacerbates ALI by increasing systemic exposure to microbial products (including circulating LPS), remodeling amino acid metabolism, and depleting microbiota-derived protective metabolites[41,42]. In germ-free (microbiota-depleted) mice, RrNVs retained a certain degree of protective effect, suggesting a partially intrinsic anti-inflammatory capacity independent of the microbiota. However, the stronger protective effect conferred by FMT from RrNVs-treated donors indicates that its action is also dependent on gut microbiota remodeling. This finding is consistent with accumulating evidence that microbiota-derived metabolites, such as short-chain fatty acids (SCFAs), tryptophan metabolites, and bile acid derivatives, serve critical functions in regulating susceptibility to ALI[43,44].

In the RrNVs regulatory network, citrate and cyclohexane-related metabolites were identified as key metabolic nodes, consistent with their regulatory effects on the gut microbiota and its metabolome[45]. RrNVs promote microecological homeostasis, attenuate inflammatory signaling, and limit the shunting of tryptophan toward the kynurenine pathway by reducing the abundance of LPS-producing bacteria and enriching beneficial microbiota[46,47]. This restored microbial activity further remodels carbon and lipid metabolism, leading to elevated levels of citrate and cyclohexane-related metabolites. These metabolites, associated with immunometabolic reprogramming, may further inhibit overactivation of the kynurenine pathway through mechanisms involving the NF-κB signaling pathway[48,49]. These results indicate that RrNVs coordinately regulate the inflammatory response along the gut–lung axis via the

"microbiota–metabolite–tryptophan axis," thereby achieving systemic immune regulation and exerting protective effects against ALI.

Although the above findings support the multi-target immunomodulatory properties of RrNVs, several mechanistic questions remain to be addressed before their further development into a dietary intervention for ALI. Although the data from this study support the involvement of the gut–lung axis and suggest a role for microbiota-related metabolites in the immunometabolic regulation of the tryptophan–kynurenine pathway, the molecular basis underlying the interaction between RrNVs and specific bacterial taxa remains to be further investigated. Future studies should further elucidate the bidirectional interaction mechanisms between RrNVs and bacteria, including their active vesicle components, corresponding bacterial receptors and uptake pathways, regulated bacterial genetic programs, and the causal relationships between these processes and host nutritional and immune outcomes..

5. Conclusions

In summary, RrNVs provide robust protection against LPS-induced acute lung injury through multiple synergistic mechanisms. Oral administration of RrNVs inhibits excessive inflammatory responses, modulates macrophage polarization and neutrophil recruitment, and restores endothelial barrier function. Integrated metabolite–target network analysis further identified citrate and cyclohexane-related metabolites as core nodes in the RrNV-responsive protective network, suggesting their potential as bioactive mediators of the lung-protective effects of RrNVs. Furthermore, RrNVs treatment significantly ameliorated LPS-induced gut microbiota dysbiosis and restored metabolic pathways associated with citrate and cyclohexane-related metabolites. Simultaneously, it reversed the disordered tryptophan-kynurenine metabolism following LPS stimulation, collectively promoting immune homeostasis of the gut–lung axis. These findings establish RrNVs as a vesicle platform derived from a common edible fruit, with favorable biocompatibility, natural origin, multi-component characteristics, and multi-target bioactivity, offering a mechanistically defined

food-based strategy with substantial translational potential for ALI and other inflammatory lung diseases.

Acknowledgments

We acknowledge the Large Instrument Sharing Platform of the Scientific Research Center, Hangzhou Medical College. This research was supported by the Joint Fund of Natural Science Foundation of Zhejiang Province (ZCLQN25H2501, LKLZ25H280001), Zhejiang Health Science and Technology Plan (2025HY0048), Traditional Chinese medicine of Zhejiang province science and technology plan project (2025ZR076), Basic Scientific Research Funds of Department of Education of Zhejiang Province (KYQN2023005), Start-up funding of Zhejiang Provincial People's Hospital (ZRY2024J008), Guizhou Provincial Office of Science and Technology (Qiankehe Major [2025] 010), Guizhou Provincial Health Commission - Key Advantageous Discipline Cultivation Project in Southwest China (Neuro-Spinal-Spinal Cord Science).

Author contributions

Yan Zeng and Xiaoru Chang designed the study; Yan Zeng, Qin Chu, Ailin Wu, Le Ding, Yuanyuan Wang and Xin Zhang performed and analyzed the biological experiments; Yan Zeng and Jun Zhang conducted the literature review and drew the chemical structures; Xin Zhang, Xinyun Tu, Mengqing Zheng and Jie Wang, assisted with the animal experiments; Yan Zeng and Xiaoru Chang wrote the manuscript; Xiaozhou Mou, Weidong Pan and Zhangfeng Zhong supervised and guided the chemical analyses.

Conflicts of interest

The authors declare no conflicts of interest.

Data Availability Statement

The datasets, analysis methods, and experimental details used in this study can be obtained from the corresponding authors upon reasonable request.

References

1. Bos, L. D. J. & Ware, L. B. Acute respiratory distress syndrome: causes, pathophysiology, and phenotypes. *Lancet* **400**, 1145–1156 (2022).

2. Liu, H. et al. Acute lung injury: pathogenesis and treatment. *J. Transl. Med.* **23**, 926 (2025).

3. Meyer, N. J., Gattinoni, L. & Calfee, C. S. Acute respiratory distress syndrome. *Lancet* **398**, 622–637 (2021).

4. Fan, E., Brodie, D. & Slutsky, A. S. Acute respiratory distress syndrome: advances in diagnosis and treatment. *JAMA* **319**, 698–710 (2018).

5. Li, R., Li, J. & Zhou, X. Lung microbiome: new insights into the pathogenesis of respiratory diseases. *Signal Transduct. Target Ther.* **9**, 19 (2024).

6. Ren, Z., Zheng, Z. & Feng, X. Role of gut microbes in acute lung injury/acute respiratory distress syndrome. *Gut Microbes* **16**, 2440125 (2024).

7. Chen, C. et al. Novel insights into immune mechanisms in acute lung injury: focusing on gut microbiota and its metabolites. *Microbiol. Res.* **300**, 128279 (2025).

8. Hu, T. et al. Baicalein ameliorates SEB-induced acute respiratory distress syndrome in a microbiota-dependent manner. *Phytomedicine* **135**, 156049 (2024).

9. Wang, Y. & Chen, Y. Gut microbiota-derived metabolites in the regulation of host immune responses and immune-related inflammatory diseases. *Cell. Mol. Immunol.* **18**, 866–877 (2021).

10. Essex, M. et al. Gut microbiota dysbiosis is associated with altered tryptophan metabolism and dysregulated inflammatory response in COVID-19. *NPJ Biofilms Microbiomes* **10**, 66 (2024).

11. Xue, C. et al. Tryptophan metabolism in health and disease. *Cell Metab.* **35**, 1304–1326 (2023).

12. Yao, L. et al. Disrupted microbial tryptophan metabolism associates with SARS-CoV-2 acute inflammatory responses and long COVID. *Gut Microbes* **16**, 2429754

(2024).

13. Wang, H., Huang, Y. & Ding, D. Gut microbiota-derived tryptophan metabolites alleviate allergic asthma inflammation in ovalbumin-induced mice. *Foods* **13**, 1336 (2024).

14. Liu, H. et al. Plant-derived exosome-like nanovesicles: a novel therapeutic perspective for skin diseases. *J. Nanobiotechnology* **23**, 640 (2025).

15. Fang, X., Feng, J., Zhu, X., Feng, D. & Zheng, L. Plant-derived vesicle-like nanoparticles: a new tool for inflammatory bowel disease and colitis-associated cancer treatment. *Mol. Ther.* **32**, 890–909 (2024).

16. Wang, Y. et al. Honeysuckle-derived nanovesicles regulate gut microbiota for the treatment of inflammatory bowel disease. *Adv. Sci.* **12**, e05208 (2025).

17. Feng, Z., Huang, J., Fu, J., Li, L., Yu, R. & Li, L. Medicinal plant-derived exosome-like nanovesicles as regulatory mediators in microenvironment for disease treatment. *Int. J. Nanomedicine* **20**, 8451–8479 (2025).

18. Li, X. et al. Rosa Roxburghii Tratt fruit extract prevents DSS-induced ulcerative colitis in mice by modulating the gut microbiota and the IL-17 signaling pathway. *Nutrients* **15**, 4560 (2023).

19. Yang, H., Zhao, Y., Zhang, R., Zhao, L., Yang, H. & Liao, X. CiLi (Rosa roxburghii Tratt.) polyphenols improve colitis via gut microbiota-lipid mediator-immunity axis. *Food Res. Int.* **209**, 116257 (2025).

20. Huang, D. et al. Identification of polyphenols from Rosa roxburghii Tratt pomace and evaluation of in vitro and in vivo antioxidant activity. *Food Chem.* **377**, 131922 (2022).

21. Liu, Y. et al. A proanthocyanidins-rich Cili (Rosa roxburghii) fruit extract protects CCl4-induced mouse hepatic fibrosis via modulation of ferroptosis and gut microbiota. *Nutrients* **17**, 3463 (2025).

22. Xiang, L. J., Zhang, S., Luo, M. L., Long, X. X., Zhou, Y. & Yin, X. Biological activities of constituents from Rosa roxburghii and their mechanisms based on network pharmacology and biological verification. *Int. J. Mol. Sci.* **26**, 1353 (2025).

23. Zhou, H. et al. Rosa roxburghii fermentation broths attenuate bleomycin-induced pulmonary fibrosis by activating the Nrf2/HO-1/NQO1 signaling pathway and modulating gut microbiota. *Food Sci. Nutr.* **13**, e70105 (2025).

24. Chen, Z. et al. Rosa roxburghii fermented juice mitigates LPS-induced acute lung injury by modulation of intestinal flora and metabolites. *Front. Microbiol.* **15**, 1447735 (2024).

25. Zhang, M. et al. Edible ginger-derived nanoparticles: a novel therapeutic approach for the prevention and treatment of inflammatory bowel disease and colitis-associated cancer. *Biomaterials* **101**, 321–340 (2016).

26. Shi, R., Tan, W., Jin, H. et al. MicroRNA-enriched plant-derived exosomes alleviate colitis by modulating systemic immunity, metabolic homeostasis, and gut microbiota. *Adv. Sci.* **12**, e05921 (2025).

27. Wang, L., Li, Y., Xia, R. et al. Component analysis and anti-pulmonary fibrosis effects of Rosa sterilis juice. *Food Funct.* **13**, 12915–12924 (2022).

28. Li, Z. et al. A multifunctional nanoparticle mitigating cytokine storm by scavenging multiple inflammatory mediators of sepsis. *ACS Nano* **17**, 8551–8563 (2023).

29. Liu, Y., Xu, R., Gu, H. et al. Metabolic reprogramming in macrophage responses. *Biomark. Res.* **9**, 1 (2021).

30. Zhao, Y., Zhu, X., Hu, L. et al. Macrophage membrane-coated polydopamine nanomedicine for treating acute lung injury through modulation of neutrophil extracellular traps and M2 macrophage polarization. *Mater. Today Bio* **25**, 101708 (2025).

31. Yang, J., Huang, X., Yu, Q. et al. Extracellular vesicles derived from M2-like

macrophages alleviate acute lung injury in a miR-709-mediated manner. *J. Extracell. Vesicles* **13**, e12437 (2024).

32. Jing, C., Castro-Dopico, T., Richoz, N. et al. Macrophage metabolic reprogramming presents a therapeutic target in lupus nephritis. *Proc. Natl. Acad. Sci. USA* **117**, 15160–15171 (2020).

33. Arnold, P. K., Jackson, B. T., Paras, K. I. et al. A non-canonical tricarboxylic acid cycle underlies cellular identity. *Nature* **603**, 477–480 (2022).

34. Chakrabarty, R. P. & Chandel, N. S. Mitochondria as signaling organelles control mammalian stem cell fate. *Cell Stem Cell* **28**, 394–483 (2021).

35. Sahu, U., Villa, E., Reczek, C. R. et al. Pyrimidines maintain mitochondrial pyruvate oxidation to support de novo lipogenesis. *Science* **383**, 1484–1492 (2024).

36. Yang, Z., Nicholson, S. E., Cancio, T. S., Cancio, L. C. & Li, Y. Complement as a vital nexus of the pathobiological connectome for acute respiratory distress syndrome: an emerging therapeutic target. *Front. Immunol.* **14**, 1100461 (2023).

37. Han, X., Alameh, M. G., Butowska, K. et al. Adjuvant lipidoid-substituted lipid nanoparticles augment the immunogenicity of SARS-CoV-2 mRNA vaccines. *Nat. Nanotechnol.* **18**, 1105–1114 (2023).

38. Zhang, J., Zhang, M., Zhang, W. H. et al. Total flavonoids of Inula japonica alleviated the inflammatory response and oxidative stress in LPS-induced acute lung injury via inhibiting the sEH activity: insights from lipid metabolomics. *Phytomedicine* **107**, 154380 (2022).

39. Zhang, J., Zhang, M., Zhang, W. H. et al. Total terpenoids of Inula japonica activated the Nrf2 receptor to alleviate the inflammation and oxidative stress in LPS-induced acute lung injury. *Phytomedicine* **107**, 154377 (2022).

40. Zhang, J., Zhang, M., Zhu, Q. M. et al. Allosteric regulation of Keap1 by β-hydroxy-α-cyclocostunolide for the treatment of acute lung injury. *Acta Pharm. Sin. B* **14**, 4174–

4178 (2024).

41. Medina-Rodriguez, E. M., Madorma, D., O'Connor, G. et al. Identification of a signaling mechanism by which the microbiome regulates Th17 cell-mediated depressive-like behaviors in mice. *Am. J. Psychiatry* **177**, 974–990 (2020).

42. Zhang, F., Lau, R. I., Liu, Q., Su, Q., Chan, F. K. L. & Ng, S. C. Gut microbiota in COVID-19: key microbial changes, potential mechanisms and clinical applications. *Nat. Rev. Gastroenterol. Hepatol.* **20**, 323–337 (2023).

43. Huang, J., Liu, D., Wang, Y. et al. Ginseng polysaccharides alter the gut microbiota and kynurenine/tryptophan ratio, potentiating the antitumour effect of antiprogrammed cell death 1/programmed cell death ligand 1 (anti-PD-1/PD-L1) immunotherapy. *Gut* **71**, 734–745 (2022).

44. Subhash, A., Bamigbade, G., Jarusheh, H. et al. Characterization, biofunctionalities, and in vitro gut microbiota modulation of nanoparticles polysaccharides ultrasonically extracted from date seeds. *Int. J. Biol. Macromol.* **310**, 143120 (2025).

45. Wang, Q., Zhao, H., Bekele, T. G., Qu, B. & Chen, J. Citric acid can enhance the uptake and accumulation of organophosphate esters (OPEs) in Suaeda salsa rhizosphere: potential for phytoremediation. *J. Hazard. Mater.* **443**, 130169 (2023).

46. Campesato, L. F., Budhu, S., Tchaicha, J. et al. Blockade of the AHR restricts a Treg-macrophage suppressive axis induced by L-Kynurenine. *Nat. Commun.* **11**, 4011 (2020).

47. Zhang, Y., Tu, S., Ji, X. et al. Dubosiella newyorkensis modulates immune tolerance in colitis via the L-lysine-activated AhR-IDO1-Kyn pathway. *Nat. Commun.* **15**, 1333 (2024).

48. Jiang, Z. M., Wang, F. F., Zhao, Y. Y. et al. Hypericum perforatum L. attenuates depression by regulating Akkermansia muciniphila, tryptophan metabolism and NFκB-NLRP2-Caspase1-IL1β pathway. *Phytomedicine* **132**, 155847 (2024).

49. Li, R., Liu, Y., Li, G. et al. Chebulinic acid from Chebulae fructus alleviates influenza virus-induced acute lung injury by inhibiting IDO1-Kyn axis activation. *Phytomedicine* **148**, 157362 (2025).

Supplementary Files

This is a list of supplementary files associated with this preprint. Click to download.

- SupplementaryMaterials.docx